Check for updates

Proceedings of the ASME 2026 45th International Conference on Ocean, Offshore and Arctic Engineering
OMAE2026
June 7-12, 2026, Tokyo, Japan

OMAE2026-175426

Downloaded from asmedigitalcollection.asme.org/OMAE/proceedings-pdf/OMAE2026/89596/V010T14A005/7645839/v010t14a005-omae2026-175426.pdf by Deutsches Zentrum für Luft- und Raumfahrt (DLR) user on 19 October 2026

THE IMPACT OF INCORPORATING REALISTIC INFLOW IN ASSESSING HYDROGENERATOR PERFORMANCE FOR A WASP VESSEL

Lars Schmitz*,†, Annika Fitz†, Cedric Fallet, Tobias Lampe, Thorben Schwedt, Dheeraj Gosala, Sören Ehlers

German Aerospace Center (DLR) - Institute of Maritime Technologies and Propulsion Systems, Geesthacht, Germany

ABSTRACT

Wind-assisted ship propulsion (WASP) is a promising technology to defossilise the shipping industry and reduce dependency on volatile fuel prices, while ensuring an economic ship operation. Ships designed to primarily use wind propulsion can, in favourable conditions, travel at speeds higher than required by the routing or targeted arrival time. In such cases, hydrogenerators can salvage the excess energy to power the hotel load or for propulsion during periods of low wind.

To form a compelling business case, it's critical to correctly assess the ship's and hydrogenator's performance in realistic conditions. WASP ships operate at a constant drift and heel angle, which, combined with the hydrogenerator's proximity to the hull, creates an oblique and highly inhomogeneous inflow. This paper evaluates the impact of realistic inflow conditions on the performance of a dual hydrogenerator system on a sailing cargo ship.

Relevant operation conditions, based on long-term North Atlantic routing data, are modeled with RANSE-CFD to extract the complex flow field. These findings are then integrated into the QBlade turbine modeling software to simulate the actual turbine geometry and the flow around it. The research quantifies the differences in turbine power output and drag between a realistic, inhomogeneous flow field and a homogeneous one. This enables to efficiently assess the effect of realistic inflow, ensuring reliable performance prediction and consequently enables optimal generator placement.

Keywords: Wind propulsion, WASP, Decarbonisation, Hydrogeneration, Oblique Flow

1. INTRODUCTION

There is a push to green technologies in the shipping industry, as it faces geostrategic challenges and mounting regulatory pressure from CII, FuelEU, EU ETS and IMO Codes, alongside the rise of emission control areas and green corridors [1–4]. While alternative fuels offer long-term decarbonisation potential, major challenges remain in availability, energy density, bunkering infrastructure and price volatility [5]. Wind propulsion for ships emerges as a complementary solution, with the potential to provide a majority of ship thrust in specific cases. The technology leverages inexhaustible wind energy to reduce or replace fuel demand, lower emissions and enhance regulatory compliance [4, 6–9]. Beyond high potential fuel savings, wind propulsion technology also reduces dependence on fossil fuel supply chains, thus increasing the economies resilience to geopolitical challenges, improves sea-keeping behaviour also for wind-assisted ships[10], supports or enables operation in emission control zones and green corridors and offers a significant public relations advantage. With 77 operational vessels employing wind propulsion [11] in 2025, Wind propulsion demonstrates maturity and operational viability [12].

Ships with large sail areas, which aim for a high percentage of sailing operation [13, 14] or solely employ wind propulsion [15], invariably will feature a variable operational and speed profile with high achieved sailing speeds in favourable wind areas and slower speeds if the wind is not in favour. For these ships, it may be sensible to employ hydrogenerators to make use of excess power during high speed passages, which can be stored and used at a later stage [15, 16].

While the technology represents a substantial potential for energy regeneration, performance of the hydrogenerators and overall impact on ship performance should be carefully monitored. Current performance assessments of hydrogenerators often rely on simplified homogeneous inflow speed [16, 17]. However, ships employing wind propulsion operate under constant drift and heel [18–20], which results in a complex, oblique and inhomogeneous inflow field on the propeller, but also at the hy-

†Joint first authors
*Corresponding author: lars.schmitz@dlr.de
Documentation for `asmeconf.cls`: Version 1.43, March 9, 2026.

Copyright © 2026 by ASME; reuse license CC-BY 4.0

drogenerator [21]. It has been shown, that oblique inflow to a propeller influences its behaviour, with possible adverse or beneficial effects on its efficiency [22–26] and similar effects may be suspected for hydrogenerators, especially in a dual configuration, with a turbine on the port and starboard side. The goal of this paper is to quantify the performance impact of realistic oblique inflow on hydrogenerators, as typically experienced on a wind propulsed cargo ship including leeway and heel. The turbine output power and torque are analysed for a dual submersible hydrogenerator setup. Additionally, the aspects influencing optimal placement are discussed as well as the benefit of using the proposed methodology to optimise placement in the future. While previous studies have acknowledged the presence of oblique flow due to drift and heel [19, 21] and the impact of drift and oblique flow on propeller efficiency [22–24], a quantitative analysis of its impact on the performance of hydrogenerators has not yet been performed. This paper aims to fill that specific gap using realistic operating conditions including drift and heel.

To achieve this, the paper is structured as follows. In Sect. 2.1 the case study used within the paper is presented and the general hydrogenerator setup is described. In Sect. 2.2, the definition of the employed operating conditions, extracted from routing results are described. In Sect. 2.3 the methodology to simulate and extract the realistic inflow conditions via CFD simulations is outlined, before the performance modelling of the hydrogenerators via *QBlade* is explained in Sect. 2.4. The results of the analysis are shown in Sect. 3 before the interpretation of the performance impact and also the implications for performance modelling and ship design are discussed in Sect. 4.

2. METHODOLOGY

This section describes the steps taken to investigate the impact of realistic flow conditions on the performance of hydrogenerators for a selected case study. First we utilized our developed framework 'Odyssa' [16] for the simulation of a case study vessel with hydroturbines, operating on a North-Atlantic route with different start dates and optimized operations. From the operation simulation we extracted relevant operating points including leeway and heel angle. For the identified operating points CFD simulations were performed to extract the inhomogeneous inflow fields of the turbines in high-resolution on port and starboard. Last we utilized the turbine simulation software *Qblade* to study the interaction of the rotor with inhomogeneous flow field. This allowed us to gain detailed insights on performance and operational conditions of hydroturbines in this set-up.

2.1. Case Study Definition

The reference vessel of this study (see Fig. 1) is a 130 m sailing cargo vessel with a four-mast DynaRig by Southern Spars, a tonnage of 12 000 t, length of 130 m and a design draught of 7.9 m. The ship design is based on the Ecoliner of Dykstra Naval Architects [27]. The sailing capability was further enhanced by adding a retractable centreboard, resulting in 20.3 m draught when in operation [18]. The vessel's design is optimized for sailing at a reference speed of 10 kn, with a maximum speed capability of up to 17 kn under sail alone. The high sailing speeds allow the vessel to use hydrogenerators. In this set-up the

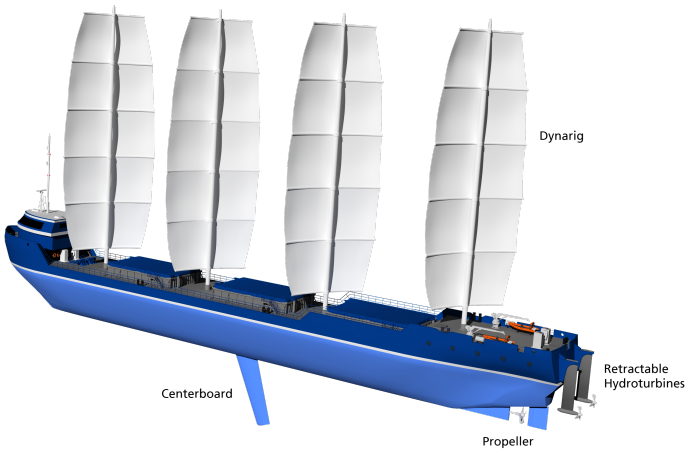


FIGURE 1: Reference vessel with retractable hydrogenerators.

position of the dual submersible hydrogenerators with a diameter of 4 m each is set to be on the transom and has been chosen with an offset of 4 m from the centreline, which provides relatively free inflow but also maximizes immersion when heeled. The vertical position has been chosen to provide a clearance between blade tips and waterline in hydrostatic condition of 1 m. The vertical and horizontal positions of hydrogenerator turbine shafts are summarized in Tab. 2. Structural considerations regarding the hydrogenerator leg design and the resistance of the leg are not considered in the current study.

For the turbine geometry we selected a design for a sports sail yacht and with a high power coefficient from [28] and scaled it to 4 m rotor diameter. The power coefficient of the turbine determines the ratio of the usable power to the power of the flow [29]. For a marine turbine of swept area A operating in sea water with density ρ and at inflow velocity V, generating the mechanical power P, the power coefficient C_P is:

$$C_P = \frac{P}{\frac{1}{2}\rho A V^3} \tag{1}$$

Since the hydrogenerator is not fixed to the seabed as a marine current turbine, the turbine drag will slow down the vessel with the drag force F_D. The turbine drag coefficient C_D is described as:

$$C_D = \frac{F_D}{\frac{1}{2}\rho A V^2} \tag{2}$$

The characteristic curves for C_P and C_D were obtained with the inbuilt Blade Element Momentum (BEM) method in *Qblade* over the tips speed ratio TSR, with the rotational speed n and the turbine diameter D:

$$TSR = \frac{n * \pi * D}{V} \tag{3}$$

Optimally, the turbine has to be operated at a rotational speed matching the vessel operating point and resulting in the best ratio of C_P to C_D. Since the turbines are positioned in a twin set-up behind the vessel stern, the reduction of the inflow velocity was approximated with the wake fraction for twin-screw vessels w_t

Copyright © 2026 by ASME; reuse license CC-BY 4.0

Downloaded from asmedigitalcollection.asme.org/OMAE/proceedings-pdf/OMAE2026/89596/V010T14A005/7645839/v010t14a005-omae2026-175426.pdf by Deutsches Zentrum für Luft- und Raumfahrt (DLR) user on 19 October 2026

based on the ships block coefficient C_B, length L and breadth B as proposed by Harvald and described in [30]:

$$w_t = (0.71 - 2.39C_B + 2.33C_B^2) + (0.12C_B^4(6.5 - L/B)) \quad (4)$$

The vessel and turbine design were integrated in the power prediction program (PPP) of the windship simulation framework Odyssa [16]. In Odyssa the forces of the sails, hull, propeller and hydrogenerators are balanced in a 4-DOF equilibrium solver for all relevant operating conditions of ship speed, wind speed, wind angle of attack, sea wave height and sea wave angle of attack. The results are collected in the response matrix, representing the full range of operating points of the vessel.

2.2. Definition of Realistic Operating Conditions

To identify the most relevant operating points of recuperation and inflow conditions of the hydrogenerators for further investigation the route simulation module of Odyssa was applied. The vessel operation was simulated on the route of Hamburg to New York for various start dates, under progressing weather conditions and a voyage time of 20 days, which corresponds to approximately 7 kn average vessel speed. An energy optimization algorithm was applied, identifying the most energy efficient route per voyage including recuperation energy [31]. Figure 2 illustrates various crossings with different courses taken according to the optimal energy harvest by the hydrogenerators.



FIGURE 2: Route simulation of the model ship on a route from Hamburg to New York with energy optimized path and vessel speed for various start dates.

The simulation allowed us to determine the operating points in recuperation mode at which the vessel operated for the majority of the time. Table 1 shows the selected operating conditions, which represent 13.5 % of total vessel operation time (Op.) and 16.3 % of the time spent in recuperation mode (Recup.). Furthermore, by focusing on a single vessel speed and varying the drift conditions, the sole influence of drift on hydrogenerator efficiency can be analysed. The identified drift and speed values serve as input for the further investigation of the flow field around the hull in CFD.

2.3. Modelling of Realistic Inflow Conditions

Based on the results from the PPP and routing simulations, representative operational cases as described in Tab. 1 have been chosen. RANSE-CFD has been employed to model the flow

TABLE 1: Identified relevant operating conditions with drift and hydrogeneration

Speed [kn] ±0.5	Drift [°] ±0.25	Heel [°] ±0.25	Op.[%]	Recup.[%]
	0	−1	1.1	1.1
	1	−3	4.4	5.3
11	2	−6	4.9	6.2
	3	−9.5	3.1	3.6
	4	−11	0.1	0.1
			13.5	**16.3**

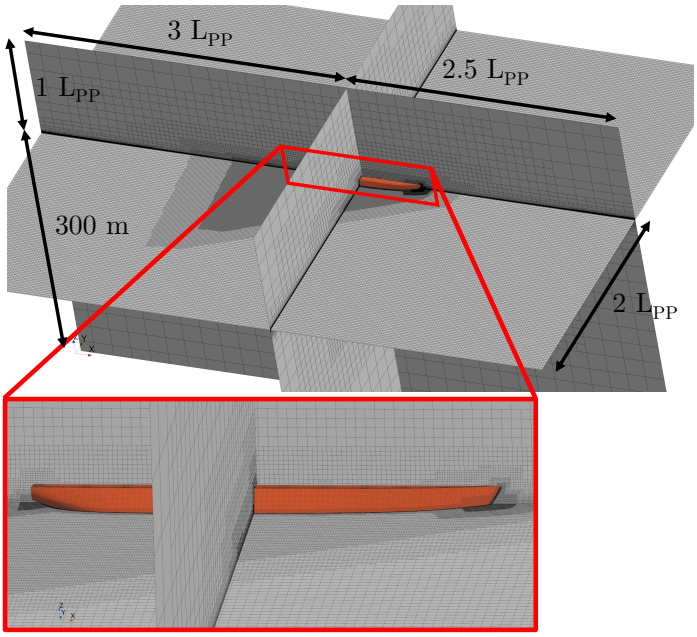


FIGURE 3: Background mesh and refinements with domain dimensions.

around the ship in these conditions to extract realistic inflow fields for the hydrogenerators. The commercial finite-volume CFD code *STAR-CCM+* was used to simulate the calm-water resistance cases including drift and heel. While the mesh varies slightly, the setup was identical for each case and the mesh was adapted to the differing inflow conditions. The base settings, are in line with best practice recommendations from ITTC [32, 33] and the *STAR-CCM+* user guide [34]. The simulations have been set up as unsteady simulations with a first order temporal discretisation to obtain a steady-state simulation, as recommended in [32, 33], utilizing the Volume of Fluid (VOF) approach to resolve the free surface. To avoid smearing of the free surface, the High Resolution Interface Capturing (HRIC) scheme is applied [35]. For turbulence modelling, the $k - \omega$ *SST* model was employed [36]. Drift angle and heel angle have been imposed as indicated in Tab. 1, while the ship was free to heave and trim. To stabilize the simulation and accelerate convergence, a ramp was employed on the flow speed and on the introduction of forces through the body motion solver. The computational domain has been set up as presented in Fig. 3 with a forcing

Downloaded from asmedigitalcollection.asme.org/OMAE/proceedings-pdf/OMAE2026/89596/V010T14A005/7645839/v010t14a005-omae2026-175426.pdf by Deutsches Zentrum für Luft- und Raumfahrt (DLR) user on 19 October 2026

Copyright © 2026 by ASME; reuse license CC-BY 4.0

TABLE 2: Positions of hydrogenerator shaft lines positioned in centre of extracted wake field.

Identifier	Pos_x [m]	Pos_y [m]	Pos_z [m]
Transom port	−63.0	4.0	−3.2
Transom starboard	−63.0	−4.0	−3.2

approach to dampen disturbances towards the domain boundaries. The boundary layer is modelled through a wall function approach with cell sizes at the ship surface leading to an average value of $y+ = 100$. Grid refinements to resolve the free surface and relevant hull features have been employed, also see Fig. 3. The simulations were assumed to be converged once residuals, specifically describing momentum and turbulent kinetic energy have dropped by some orders of magnitude and no change in position (heave and trim) nor in forces and moments could be observed over some iterations. Simulations have been run over 200 s of physical time, after which these conditions have always been satisfied.

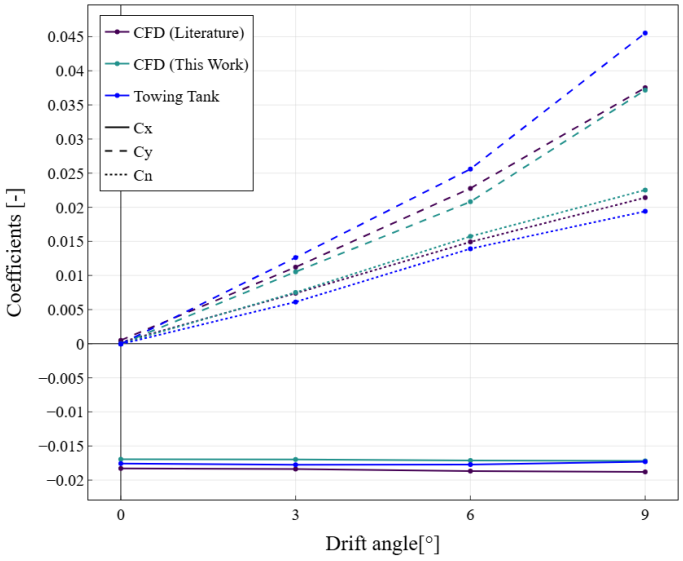


FIGURE 4: Validation results for KVLCC2M at drift for drag coefficient C_x, lift coefficient C_y and moment coefficient C_n. Our simulation setup compared to towing tank tests [37] and CFD results from literature [38].

The simulation setup for drift has been validated through comparison to model tests [37] and simulation results [38] for the KVLCC2M tanker hull at drift, achieving similar error margins for the forces as [38], see Fig. 4.

The inflow field for the hydrogenerator is extracted from the converged CFD simulations by means of velocity vectors in x, y and z in the ship coordinate system. The origin is placed in the centre of gravity, which is at $x = 63.0$ m in relation to the transom, on centre line and at $z = 0.2$ m above the waterline. The x axis is aligned with the ship centre line and positive in ship forward direction, the y axis is positive to port side and the z axis is positive in the upward direction, as shown in Fig. 3. An equally spaced grid of the wake for the further use in *QBlade*, compare Sect. 2.4, is extracted for each potential hydrogenerator position, see Sect. 2.1 through a presentation grid in *STAR-CCM+*. This approach has the advantage of using all information available within the numerical simulation for resampling and interpolation. Two different positions, as defined in Tab. 2 were extracted for further use in the performance modelling of the hydrogenerators.

2.4. Hydrogenerator Performance Modelling

To investigate the interaction of the hydrogenerator with the experienced flow field behind the ship's hull at different drifts and heels, we employ the software *QBlade*. *QBlade* is a multi-physics code solving aero-, hydro- and structural dynamic interactions. It is originally designed for wind turbines but can be applied to marine turbines by adjusting the fluid parameters from air to sea water, as applied in [39, 40]. The aerodynamics, respectively in our case hydrodynamics, of the fluid-rotor interaction are modelled with a Lifting Line Free Vortex Wake Method (LLFVW) [41, 42]. The turbine wake is modelled through Lagrangian vortex elements, which improves the spatial and temporal resolution compared to the blade element method (BEM), which restrains the shape of the wake [43]. The method allows fast computation of turbine performance under inhomogeneous inflow conditions. We extracted cutplanes of the CFD flow field with the assumption, that the interaction of the flow field around the hull is not affected by the turbine. Furthermore, that the change in turbine drag from homogeneous to inhomogeneous inflow does not significantly affect the overall vessel force balance, and the selected operating points therefore remain valid. The extracted cutplanes from CFD are converted to the turbsim binary windfield format [44] with the Openfast Toolbox [45] as a steady wind field with a inhomogeneous velocity distribution. Figure 5 shows an example simulation of the starboard hydroturbine in *QBlade*. The rotor is modelled with blade sections of the Wortman FX 63-137 as proposed by [28] and scaled to 4 m. For the port side the original direction of rotation is kept, while it is reversed for the starboard side to generate a contra-rotating pair of turbines. To simulate under water conditions the environment is set to 'Onshore' but with sea water density of 1025 kg m^{-3} and a kinematic viscosity of 1.307×10^{-6} m^2 s^{-1}, as recommended by the *QBlade* documentation [42]. The simulation length is 10 s with a time step of 0.005 s. For each simulation the rotational speed is adjusted to obtain a tip speed ratio of 2.2, mimicking a simplified TSR controller and resulting in a similar average C_P value of 0.42 for all simulations. The dynamics of the controller are not modelled since the inflow field is inhomogeneous but steady. Since we used the *QBlade* Community Edition for this study, the geometric model of the gondola cannot be adjusted. Therefore, in the simulation, the tower drag, here equivalent to the drag of the hydrogenerator leg, is deactivated.

3. RESULTS

In this section, the results of the conducted analysis are presented with regard to the observed differences in the flow field and a comparison of the attained hydrogenerator performances.

Downloaded from asmedigitalcollection.asme.org/OMAE/proceedings-pdf/OMAE2026/89596/V010T14A005/7645839/v010t14a005-omae2026-175426.pdf by Deutsches Zentrum für Luft- und Raumfahrt (DLR) user on 19 October 2026

Copyright © 2026 by ASME; reuse license CC-BY 4.0

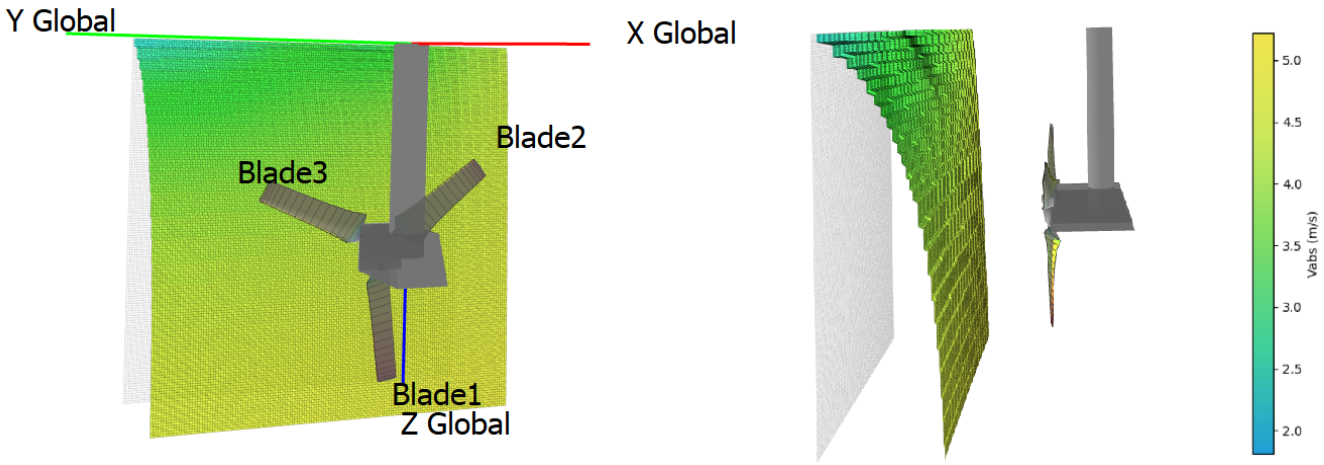


FIGURE 5: *QBlade* Simulation of the starboard hydrogenerator with an inhomogeneous inflow field at 0° drift and 1° heel angle.

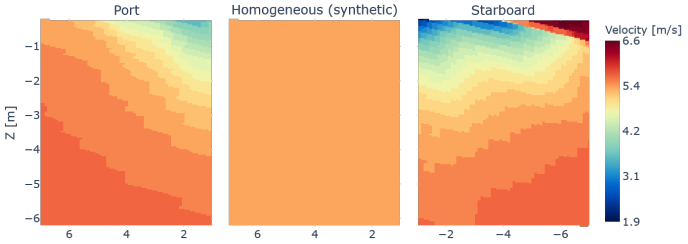


FIGURE 6: Velocity magnitudes of inflow to port and starboard turbine at 11 kn ship speed with 4° drift and –11° heel in direct comparison to a synthetic homogeneous inflow field assuming a wake fraction of 0.13.

3.1. Characterization of Inflow Field

The *StarCCM+* CFD simulations, as described in Sect. 2.3 were performed for the operating conditions as shown in Tab. 1 to simulate realistic inflow based on the experienced sailing conditions en-route, compare Sect. 2.1. As described in Sect. 2.3, the inflow velocities to the hydrogenerators were captured from the simulations. A visualisation for the case of 11 kn ship speed, 4° of drift and −11° heel, showing the converged state of the simulation, the deformed free surface including iso lines for visualisation of the surface elevation, streamlines around the hull and the inflow speeds on a 6 m × 6 m plane centred around the hydrogenerator shafts on port and starboard is shown in Fig. 7. A more detailed comparison for the inhomogeneous inflow on port, starboard and a homogeneous inflow with equivalent speed can be seen in Fig. 6. Only total velocity magnitudes are depicted. The influence of the boundary layer around the hull is indicated by the low speed area towards the top of both vector fields. Also the influence of heel is visible through the diagonal speed distribution. Additionally, part of the plotted vector field on the starboard side protrudes through the free surface. It should be noted, that the plotted vector field is 6 m × 6 m and thus much larger than the 4 m diameter of the turbines. The flow velocities between the flow fields on port and starboard differ by up to 3.45 m s^{-1}, which is equivalent to 60.1 % of ship speed. When comparing with the reference velocity, which is ship speed corrected for the wake fraction of 0.13 with 4, the average speeds for port and starboard differ by 1.3 % and 6.1 % respectively, but the minimal experienced speed is up to 61.7 % lower and the maximum speed is 8.14 % higher than the reference velocity. These differences between reference flow speed and the actually experienced speeds also justifies a deeper analysis of the attained hydrogenerator performance in the following section.

3.2. Hydrogenerator Performance Comparison

The *QBlade* simulations, described in Sect. 2.4 were performed for all operating conditions as shown in Tab. 1. Furthermore, we simulated a reference case with a homogeneous inflow field and the assumption of an inflow speed with a wake fraction of 0.13 on the ship speed of 11 kn based on Eq. 4. Figure 8 shows the *QBlade* LLFVW simulation results of mechanical power at the turbine shaft with homogenous inflow and the applied wake fraction (Ref_wakefrac) of Eq. 4 and operating points with inhomogenous inflow at leeway (L) and heel angle (H) for each ship side. After seven seconds the simulation is stabilized. Compared to the results of the routing stage, which applied BEM, (Ref_wakefrac) with LLFVW shows a 1.3% increase in the power output, which might be caused by the different approaches of modelling the wake. Still the results are close to each other. By incorporating realistic inflow conditions the power output of the turbine decreases by 5.2 % on average over all simulations compared to the BEM results of the routing stage and 6.5 % compared to (Ref_wakefrac).

Except for the port side turbine in the 4° leeway and −11° heel case (L4_H11_Port), which yielded a higher power output. Nevertheless, the approximation by the wake fraction remains reasonable when compared with free-flow operation at 11 kn (Ref_freeflow, which would yield a turbine power output of 506 kW and corresponds to a 64.3 % overestimation of power. The operating cases without leeway, but a small heel angle of −1° (L0_H1_Port and L0_H1_Starb) show a slight advantage of the starboard compared to the port side turbine with an average power output of 365 kW and 360 kW, respectively. This effect is negated for all operating cases with leeway, where the port side turbine (solid lines) experiences a higher average inflow speed than the

Downloaded from asmedigitalcollection.asme.org/OMAE/proceedings-pdf/OMAE2026/89596/V010T14A005/7645839/v010t14a005-omae2026-175426.pdf by Deutsches Zentrum für Luft- und Raumfahrt (DLR) user on 19 October 2026

Copyright © 2026 by ASME; reuse license CC-BY 4.0

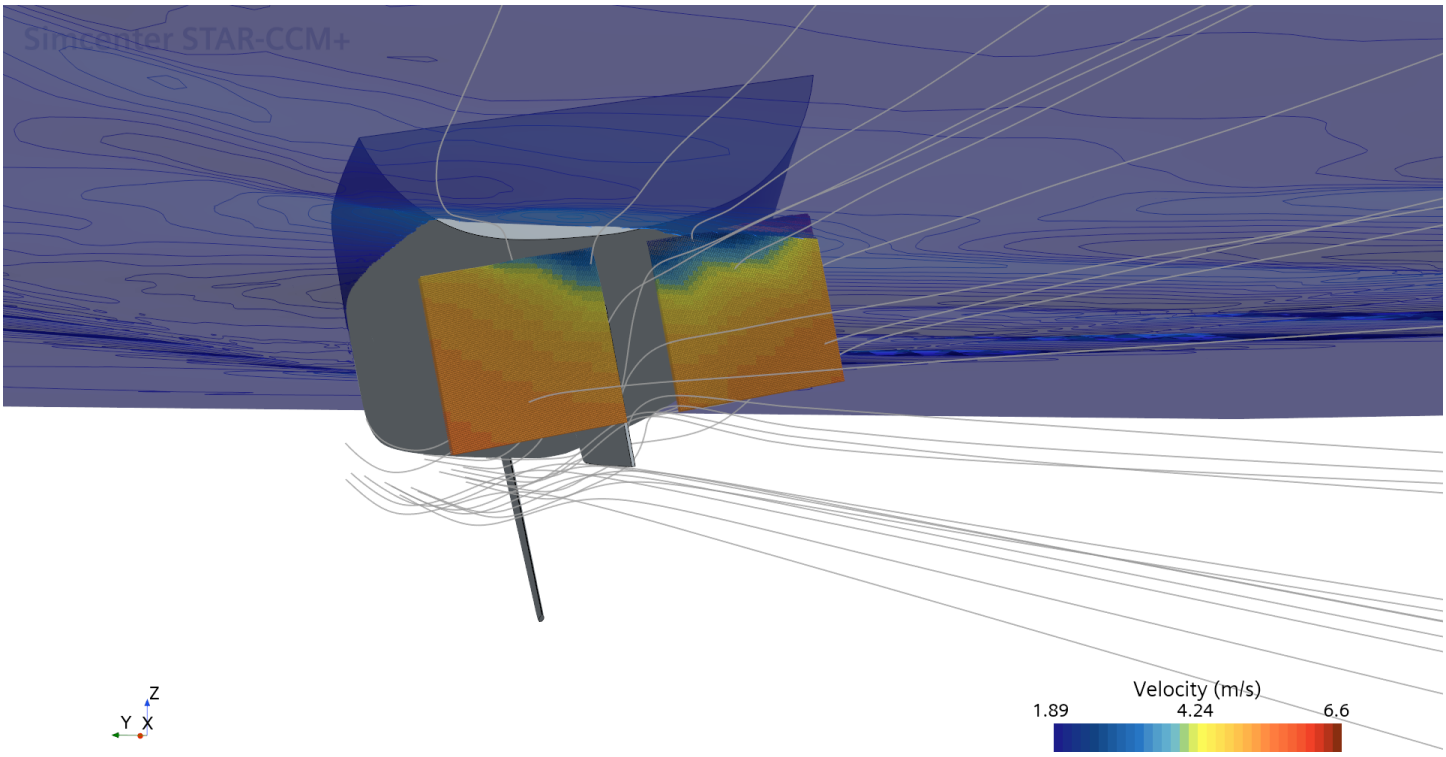


FIGURE 7: Visualisation of inflow to port and starboard turbine at 11 kn ship speed with 4° drift and −11° heel. Presentation grid shows velocities on a 6 m × 6 m plane with a turbine diameter of 4 m, positioned it its centre (not shown). Free surface including iso lines showing surface elevation and streamlines around the hull shown.

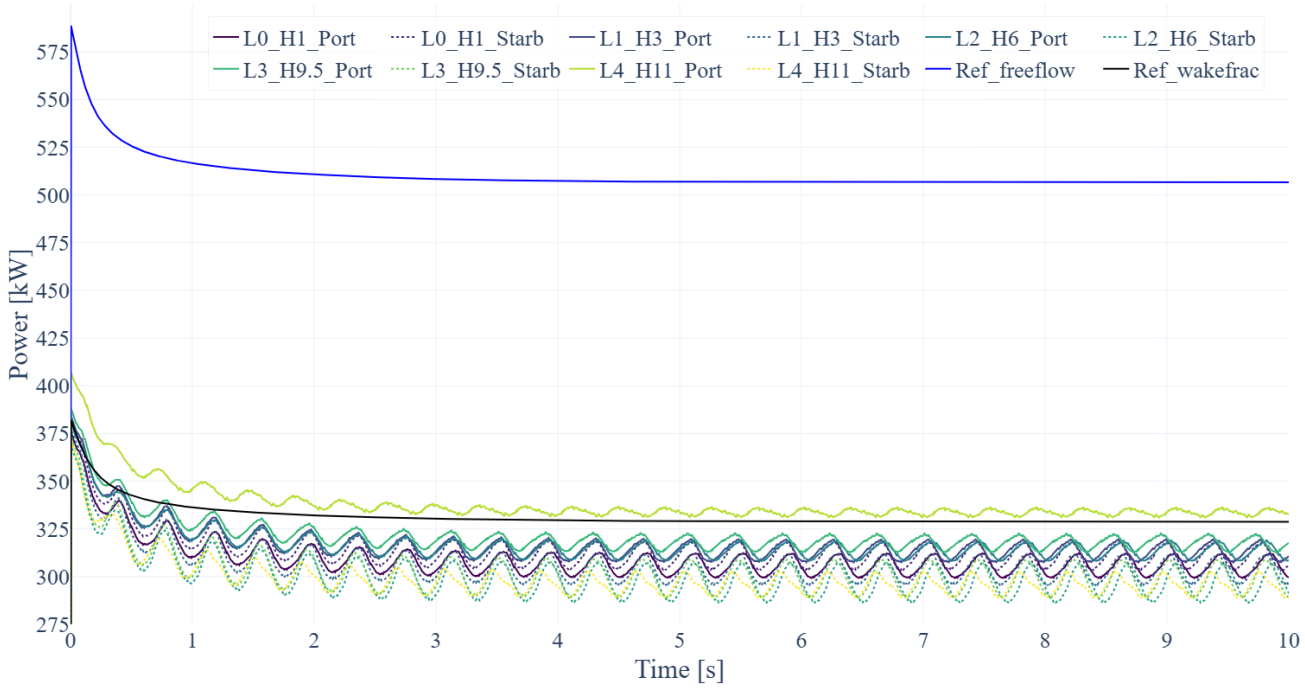


FIGURE 8: *QBlade* Simulation of the mechanical power generated at the turbine shaft at 11 kn ship speed and inhomogeneous inflow at different leeway (L) and heel (H) angles in degrees, generated by the port side (Port) and the starboard (Starb) hydrogenerator. As a comparison a hydrogenerator operating under homogeneous inflow conditions at ship speed (Ref_freeflow) and with a wake fraction of 0.13 is shown (Ref_wakefrac).

Downloaded from asmedigitalcollection.asme.org/OMAE/proceedings-pdf/OMAE2026/89596/V010T14A005/7645839/v010t14a005-omae2026-175426.pdf by Deutsches Zentrum für Luft- und Raumfahrt (DLR) user on 19 October 2026

Copyright © 2026 by ASME; reuse license CC-BY 4.0

starboard side (dashed lines). The spread between the two sides increases with the leeway angle, reaching its maximum at the 4° leeway angle with a maximum power output delta of 47 kW in the stabilized simulation section. A high imbalance in power means also a high imbalance in drag between the turbines and following the necessity to counterbalance it with the rudder. The output power fluctuates as a repeating pattern when the rotor blades enter and leave lower speed areas of the flow field close to the hull as can be seen in Fig. 5. The fluctuation of power is stronger on the starboard side with a steeper peak-to-valley difference in inflow speed over the rotor plane. The highest torque fluctuation occurs on the 2° leeway and −6° heel case (L2_H6_Starb) with a 4.7 N m delta at a period of 0.37 s, while the flow field becomes almost homogeneous for the 4° leeway and −11° heel case on the port side (L4_H11_Port). The torque fluctuations are a potential risk of imposing vibrations and structural stress on the rotor, shaft and generator and furthermore inducing vibrations into the hull. By

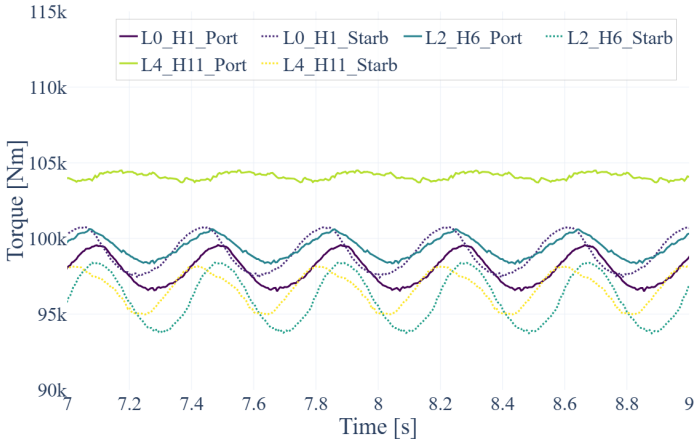


FIGURE 9: Torque fluctuation in Nm at the turbine shaft at different leeway (L) and heel angles (H) in °.

the operation with leeway angle the port side of the ship becomes more exposed to the water flow, while the starboard side experiences stronger shading. This results in an imbalance in power production between port and starboard. We performed additional simulations of the same operating points but with 0° heel angle to differentiate the impacts of heel and leeway. Figure 10 shows the relative delta in mechanical power output for the operating points with heel (purple) and without heel (green) compared to a reference value (Ref_L0_H0), corresponding to the average of starboard and port side at 0° leeway and 0° heel. The no heel curve (green), should overlap with this value for port and starboard, since the flow fields are expected to be symmetric in this operating point. Yet it shows a slight imbalance of the port and starboard side, which might be a result of a non-symmetric mesh in the CFD simulation. To the port side the turbine performance increases to 9.8 % with and 8.6 % without heel, under increasing leeway angle. On the starboard side it drops down to −2.75 % and −1.46 %, respectively. As the difference between the purple curve with heel and the green curve without heel show, the ships inclination has a negative effect on the inflow conditions, resulting in a flatter increase on the port side and a steeper decrease on the starboard side. Summed up over both turbines in this configuration, operating with a leeway and heel angle has a slightly positive effect on the total turbine performance. The increase in

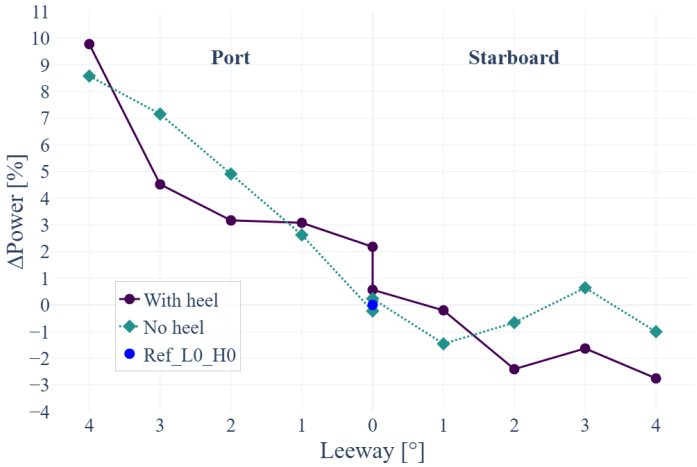


FIGURE 10: Relative change in hydrogenerator output power for port and starboard turbine over different drift conditions compared to the averaged power output for 0° leeway and heel inhomogeneous flow field (Ref_L0_H0). Curves are shown with (purple) and without (green) heel effects. The X-axis is mirrored to visualize the simultaneous power increase and decrease on each ship side.

total output can be observed in Fig. 11. The maximum positive effect in power increase compared to inhomogeneous inflow at 0° leeway and 0° heel for the curve with heel is 3.5 % at 4° leeway.

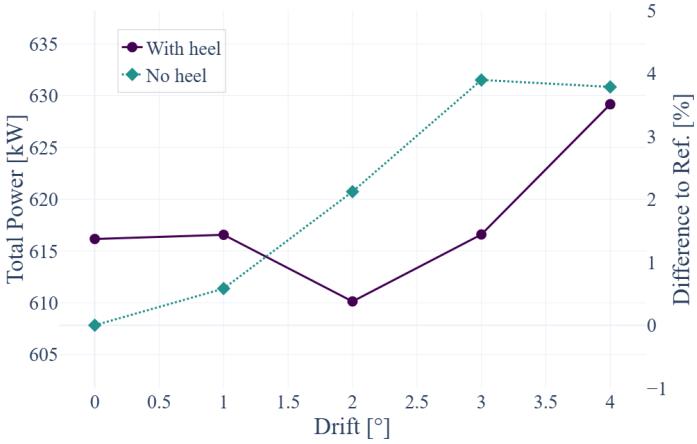


FIGURE 11: Total mechanical output power of combined port and starboard turbine at 11 kn ship speed over different drift conditions, with and without heel.

4. DISCUSSION

In this section, the results, see Sect. 3, are discussed. It is spotlighted how the performance impact through incorporating realistic inflow can be interpreted, what implications are for ship design or operation and which steps should be undertaken to generalize results and takeaways.

Downloaded from asmedigitalcollection.asme.org/OMAE/proceedings-pdf/OMAE2026/89596/V010T14A005/7645839/v010t14a005-omae2026-175426.pdf by Deutsches Zentrum für Luft- und Raumfahrt (DLR) user on 19 October 2026

Copyright © 2026 by ASME; reuse license CC-BY 4.0

4.1. Interpretation of Performance Impact

By incorporating realistic inflow conditions, we refined the performance prediction of hydroturbines in the investigated twin set-up and analysed the impact of leeway and heel conditions for each ship side. We found substantial differences in power output between the two ship sides. Yet, for the total mechanical power summed over both turbines we found a positive effect on performance with increasing drift, as the power increase on the exposed port side exceeded the deficit on the shaded starboard side. At this time, no test data is available to validate the results with measured data. However, the underlying aerodynamic part of the code has already been validated over a wide Reynolds number range, so that a fluid change from air to water does not call into question the fundamental validity of the fluid dynamic rotor characterization with *QBlade*. However, further effects, which become more relevant in water like, buoyancy, added mass or cavitation, might cause an overestimation of the power output. In the case study simulation we employed a wake fraction of 0.13 as a first assumption for the turbine inflow based on Eq. 4. On average over all investigated operating points this is 5.2 % than our *QBlade* results, with a modelled inflow field. For future work, focusing primarily on overall ship performance estimation, employing a wake fraction might still be valid. Yet, results would be improved by extracting applicable wake fractions for the relevant operating points under leeway and heel conditions from CFD inflow fields. However, to identify effects of the interaction of the turbine with the flow field such as the torque fluctuation or structural stress on the blades, modelling in *Qblade* provides a useful tool. Especially, for a dual-use set-up where a much more inhomogeneous flow field behind the skeg can be expected, it is most relevant to capture strong torque fluctuations, induced by severely shaded areas. In the simulations we applied a simplified controller, setting the turbine rotational speed to achieve an average TSR of 2.2. With an advanced controller it might be possible to balance the torque fluctuations. Additionally, it is expected, that *QBlade* provides a higher fidelity in performance and drag assessment especially for higher drift angles. Due to the fast calculation times, many different operating points and also extreme conditions could be tested in a relatively short amount of time.

4.2. Implications for Performance Modelling, Ship Design and Operation

With an observed performance implication of up to 13 % between placement on port and starboard, compare Fig. 10 for a single hydrogenerator due to drift and heel, it may be concluded to be sensible to consider realistic inflow for hydrogenerator performance. It is the key to achieve the most realistic performance prognosis and also create the opportunity to optimize positioning and alignment for maximum regeneration and minimal drag. Additionally, the observed torque fluctuations due to the operation in the inhomogeneous flow field and close to the boundary layer, Fig. 9, may induce vibrations which may be relevant in the context of fatigue. In a next step, the *QBlade* simulation could be directly linked with the CFD simulation to include also the turbine wake and refine the analysis of parasitic effects on the ship itself, for example as input to an actuator disc model.

Using the QBlade Community Edition we were not able to modify the geometry of the turbine legs and gondola, yet. Including the drag effects of these structures might reveal further implications, as for example the effect on drift, depending on the leg or gondola shape. Drawbacks of the approach are, that the surfaces, the turbines are mounted to, are not geometrically changeable. This for example would be relevant for a hydroturbine mounted directly to the ship hull. Linked to the question of parasitic drag, is the question to what extent the asymmetric power generation and drag influence the sailing equilibrium for each operation point. For assessment of the sailing performance of a ship, it is vital to correctly model the yaw balance, side force and drag components, compare [16, 18, 46]. We will assess the impact of realistic inflow on the hydrogenerators on the sail equilibrium in the operation points in a next step.

The performance differences depending on drift and heel and also the torque and power fluctuations due to the hydrogenerators operating in inhomogeneous inflow and close to the boundary layer of the ship show that the position of the hydrogenerators play an important role. For this case study, we have chosen to evaluate submersible folding hydroturbines attached to the transom, which fixes the longitudinal position and only allows to vary the offset from the centre line and vertical position. Aspects to consider include hydrodynamic efficiency with regard to the inflow, the aim to submerge the turbines also when heeled and in waves, but also structural considerations and drag created by the leg. The position on the transom limits flexibility and creates the possibility of surface piercing and reduced efficiency close to the surface, however, it also enables relatively easy retractability to reduce drag when not in use or for maintenance reasons. Hydrogenerators could also be installed as podded systems directly attached to the hull, which permanently creates drag, but ensures sufficient submersion and gives more degrees of freedom in positioning the turbines. The method, proposed in this paper, provides the possibility to assess different configurations for their power generation efficiency and induced drag, while being sufficiently fast to enable optimisation of the hydrogenerator position.

A premise in the positioning of the hydrogenerators for this study was to not protrude below base line or outside of the beam of the ship. Flow could be less disturbed further away from the hull, consequently leading to a higher power coefficient, but also increasing the risk of a collision of the generator with debris in the water. This is case specific and dependent on a risk analysis.

Potentially, the turbines could also be aligned with the flow, to maximize energy generation and minimize drag from the hydrogenerator leg. This could be done statically to have the least drag and maximum energy generation on average or dynamically to optimize each operation point individually. Our method outlined in this study can be used to analyse and optimize flow alignment by additionally introducing an active yaw of the hydrogenerators in *QBlade*. Since gondola and leg geometry and their influence on drag have not been modelled, see Sect. 2.4, which would have an substantial impact for the scenario of active alignment of the generators with the flow, this has not been done yet within the conducted study.

The case study was conducted for a bespoke sailing cargo ship with a pronounced skeg situated near the transom, see Sect. 2.1. The skeg increases ship performance in sailing op-

Copyright © 2026 by ASME; reuse license CC-BY 4.0

Downloaded from asmedigitalcollection.asme.org/OMAE/proceedings-pdf/OMAE2026/89596/V010T14A005/7645839/v010t14a005-omae2026-175426.pdf by Deutsches Zentrum für Luft- und Raumfahrt (DLR) user on 19 October 2026

eration considerably [18], however, it also realigns the flow with the ships centre line direction. Since the skeg realigns the flow, effects on hydrogenerator performance due to leeway could be smaller than observed with a more conventional design without skeg. This should be evaluated for more hull designs and also for the same hull design excluding the skeg for more general applicability.

5. CONCLUSION AND OUTLOOK

In this paper, we have presented the impact of incorporating realistic inflow in assessing hydrogenerator performance for a WASP vessel. This was achieved through a novel method, which combines weather routing, RANSE-CFD analysis and Lifting Line Free Vortex Wake (LLFVW) method. Using historical and progressing weather data, the case study ship was routed for various start dates to extract common and realistic operation points, see Sect. 2.2. Using commercial state-of-the-Art RANSE-CFD software, the realistic inflow field in the positions of the hydrogenerators was extracted for the operation points including drift and heel, see Sect. 2.3. The LLFVW method was used with the software *QBlade* to quickly model hydrogenerator performance under inhomogeneous inflow. The results were compared with a baseline case assuming a constant wake fraction. Performance differences of up to 13 % between port and starboard turbine and 6.5 % in comparison of inhomogeneous inflow to the baseline with homogeneous inflow and a standard wake fraction were reported. Additionally, it was shown that the inhomogeneous inflow leads to substantial torque and performance fluctuations which may induce vibrations.

As a next step, we will also include the effect of realistic inflow and positioning on the drag of the hydrogenerators, which will be possible with the full version of *QBlade*. As an alternative to the commercial version of *QBlade* open source frameworks as for example *OpenFAST* could be explored. To validate the method, in subsequent steps fully resolved RANSE CFD simulations should be conducted and measurement data used once available. Additionally, the method could be applied to optimise position and flow alignment of hydrogenerators to reap their full potential. Also a dual mode propeller and turbine could be considered for its efficiency through the method.

ACKNOWLEDGMENTS

The authors gratefully acknowledge the scientific support and HPC resources provided by the German Aerospace Center (DLR). The HPC system CARA is partially funded by "Saxon State Ministry for Economic Affairs, Labour and Transport" and "Federal Ministry for Economic Affairs and Climate Action". The HPC system CARO is partially funded by "Ministry of Science and Culture of Lower Saxony" and "Federal Ministry for Economic Affairs and Climate Action".

REFERENCES

[1] International Maritime Organization. "Resolution MEPC.354(78): 2022 Guidelines on the Operational Carbon Intensity Rating of Ships (CII Rating Guidelines, G4)." Resolution MEPC.354(78). International Maritime Organization, London, UK. 2022. URL https://wwwcdn.imo.org/localresources/en/KnowledgeCentre/IndexofIMOResolutions/MEPCDocuments/MEPC.354(78).pdf. Adopted on 10 June 2022.

[2] International Maritime Organization (IMO)/ Marine Environment Protection Committee. "2023 IMO STRATEGY ON REDUCTION OF GHG EMISSIONS FROM SHIPS: RESOLUTION MEPC.377(80) Annex 15." (7.7.2023). Accessed 18.12.2024, URL https://wwwcdn.imo.org/localresources/en/OurWork/Environment/Documents/annex/MEPC%2080/Annex%2015.pdf.

[3] European Parliament and the Council. "REGULATION (EU) 2023/1805 on the use of renewable and low-carbon fuels in maritime transport, and amending Directive 2009/16/EC: Reg. 2023/1805: FuelEU Maritime Regulation." (13.9./2023). Accessed 19.12.2024, URL https://eur-lex.europa.eu/eli/reg/2023/1805.

[4] Petkovic, Miro, Zubcic, Marko, Krcum, Maja and Pavic, Ivan. "Wind Assisted Ship PropulsionTechnologies – Can they Help in Emissions Reduction?" *Naše more* Vol. 68 No. 2 (2021): pp. 102–109. DOI 10.17818/NM/2021/2.6.

[5] Campbell, Michael, Eyton, Ed, MacLean, Graeme, Pons, Aleix, Scarbrough, Tim, Vasileiadis, Nikos, Wan, Justin, Endresen, Øyvind, Helgesen, Henrik, Longva, Tore, Strøm Nakstad, Ingeranne, Sekkesæter, Øyvind, Skåre, Ola Gundersen and Slotvik, Dorthe Alida Arntzen. "Study on the Readiness and Availability of Low- and Zero-Carbon Ship Technology and Marine Fuels: Full Report." (2023). URL https://greenvoyage2050.imo.org/wp-content/uploads/2023/08/Readiness-of-Low-Zero-Carbon-Marine-Fuels-Technology-Full-Report-v1.pdf. Ref. Contract No. 2022-19, RFP2022-08; Issue 3, 20 April 2023.

[6] "Applying Wind-Assisted Propulsion to ships: Energy Efficiency Retrofit Report 2024." Accessed 18.12.2024, URL https://www.lr.org/en/knowledge/research-reports/2024/applying-wind-assisted-propulsion-to-ships/.

[7] Bureau Veritas. "Technology Report: Wind Propulsion." Accessed 18.12.2024, URL https://marine-offshore.bureauveritas.com/newsroom/wind-propulsion-report.

Copyright © 2026 by ASME; reuse license CC-BY 4.0

Downloaded from asmedigitalcollection.asme.org/OMAE/proceedings-pdf/OMAE2026/89596/V010T14A005/7645839/v010t14a005-omae2026-175426.pdf by Deutsches Zentrum für Luft- und Raumfahrt (DLR) user on 19 October 2026

[8] Orestis Schinas. "REDUCTION OF GHG EMISSIONS FROM SHIPS: White paper on Wind propulsion solutions." DOI 10.13140/RG.2.2.18835.02081.

[9] Laursen, R., Patel, H., Sofiadi, D., Zhu, R., Nelissen, D., van Seters, D. and Pang, E. "Potential of Wind-assisted Propulsion for Shipping: By ABS, CE Delft & ARCSILA." Accessed 18.12.2024, URL https://emsa.europa.eu/publications/item/5078-potential-of-wind-assisted-propulsion-for-shipping.html.

[10] Bartlett, Paul. "Suction sails propel Odfjell tanker to 16% fuel savings: The power of the wind exceeded expectations and generated other unexpected benefits on a recent trans-Atlantic crossing by an Odfjell tanker." London, UK (2025). Accessed 05.01.2026, URL https://www.seatrade-maritime.com/wind-powered-ships/suction-sails-propel-odfjell-tanker-to-16-fuel-savings.

[11] International Wind Ship Association. "Wind Ship Vessel Tracker." Accessed 17.12.2025, URL https://www.wind-ship.org/vessel-tracker/.

[12] Kolodziejski, Marcin and Sosnowski, Mariusz. "Review of Wind-Assisted Propulsion Systems in Maritime Transport." *Energies* Vol. 18 No. 4 (2025): p. 897. DOI 10.3390/en18040897.

[13] Lampert, Edwin. "1.3-tonne daily fuel savings achievable with an automated wingsail: A hybrid cargo vessel equipped with four 37-m automated wing sails has reported fuel savings of 25-50% during transatlantic voyages." London, UK (2024). Accessed 5.1.2026, URL https://www.rivieramm.com/news-content-hub/news-content-hub/13-tonne-daily-fuel-savings-achievable-with-an-automated-oceanwings-wingsail-82221.

[14] Baird Maritime (ed.). "VESSEL REVIEW | Neoliner Origin – France's Neoline to deploy sailing cargo ship on trans-Atlantic routes." (2025). Accessed 5.1.2026, URL https://www.bairdmaritime.com/shipping/dry-cargo/ro-ro/vessel-review-neoliner-origin-frances-neoline-to-deploy-sailing-ro-ro-cargo-ship-on-transatlantic-routes.

[15] Grain de Sail (ed.). "Grain de Sail II." Accessed 5.1.2026, URL https://graindesail.com/en/grain-de-sail-ii/.

[16] Fitz, Annika, Gosala, Dheeraj, Gosala, Vaidehi, Lampe, Tobias, Schwedt, Thorben, Stutz, Sophie and Ehlers, Sören. "Odyssa – a techno-economic evaluation framework for wind-assisted vessels with hydrogeneration." *Ships and Offshore Structures* Vol. 0 No. 0 (2025): pp. 1–17. DOI 10.1080/17445302.2025.2529961.

[17] van der Plas, M. D., Hillege, L. and de Vos, Peter. "The impact of hydro generation on board large sailing yachts." TU Delft (ed.). *Proceedings of 15th International Marine Design Conference (IMDC-2024)*. TU Delft OPEN Publishing (2024). DOI 10.59490/imdc.2024.906. URL https://repository.tudelft.nl/record/uuid:96a8e8db-9f46-4e82-95a3-3bffe4d22498.

[18] Schmitz, Lars, Leslie-Miller, Mark, Fitz, Annika, Ehlers, Sören and Klein, Marco. "A VPP Derivative Optimisation Method for Wind-Assisted Cargo Ships Based on RANSE-CFD." Vol. Volume 7: Blue Economy Symposium; Specialty Symposium on OTEC and Correlate Devices; Smart and Sustainable Maritime Systems; Prof. Sander Calisal Honoring Symposium in Hydrodynamics, Tidal Energy, Ship Design and Education: p. V007T14A005. 2025. DOI 10.1115/OMAE2025-156594. URL https://asmedigitalcollection.asme.org/OMAE/proceedings-pdf/OMAE2025/88964/V007T14A005/7532345/v007t14a005-omae2025-156594.pdf.

[19] Gatin, Inno, Keser, Robert and Vukcevic, Vuko. "Wind Assisted Propulsion: Hidden Performance Traps." Volker Bertram (ed.). *HullPIC' 25*: pp. 134–140. 2025.

[20] van der Kolk, N. J. "Sailing Efficiency and Course Keeping Ability of Wind Assisted Ships." Dissertation, Delft University of Technology, Delft, NL. 2020. DOI 10.4233/uuid:8707309f-b9a3-4e09-916d-8fb64328a138.

[21] Hosseinzadeh, Saeed, Hudson, Dominic, R. Turnock, Stephen, Prince, Martyn and Banks, Joseph. "Influence of hull–propeller–rudder interaction on the self-propulsion of wind-assisted ships." *Physics of Fluids* Vol. 37 No. 8 (2025). DOI 10.1063/5.0281083.

[22] Schot, J. J. A. and Eggers, R. "The effect of leeway angle on the propeller performance." *Wind Propulsion 2019* (2019)DOI 10.3940/rina.win.2019.04.

[23] Wei, Xinxin, Yan, Tianhong, Sun, Tao, Liu, Shulin and Du, Hongyi. "Research on the hydrodynamic performance of propellers under oblique flow conditions." *Proceedings of the Institution of Mechanical Engineers, Part M: Journal of Engineering for the Maritime Environment* Vol. 238 No. 4 (2024): pp. 728–737. DOI 10.1177/14750902241231349.

[24] Nouroozi, Hossein and Zeraatgar, Hamid. "Propeller Hydrodynamic Characteristics in Oblique Flow by Unsteady Ranse Solver." *Polish Maritime Research* Vol. 27 No. 1 (2020): pp. 6–17. DOI 10.2478/pomr-2020-0001.

[25] Wang, Wei, Zhao, Dagang, Guo, Chunyu and Pang, Yongjie. "Analysis of Hydrodynamic Performance of L-Type Podded Propulsion with Oblique Flow Angle." *Journal of Marine Science and Engineering* Vol. 7 No. 2 (2019): p. 51. DOI 10.3390/JMSE7020051.

[26] Čalić, Ante, Jurić, Zdeslav and Katalinić, Marko. "Impact of Wind-Assisted Propulsion on Fuel Savings and Propeller Efficiency: A Case Study." *Journal of Marine Science and Engineering* Vol. 12 No. 11 (2024): p. 2100. DOI 10.3390/jmse12112100.

[27] Dykstra Naval Architects. "WASP (Ecoliner)." (29.12.2025). Accessed 29.12.2025, URL https://www.dykstra-na.nl/designs/wasp-ecoliner/.

[28] Ekinci, Serkan and Alvar, Mustafa. "Horizontal Axis Marine Current Turbine Design for Wind-electric hybrid Sailing." *Brodogradnja* Vol. 68 No. 2 (2017): pp. 127–151. DOI 10.21278/brod68209.

[29] Betz, A. "The Maximum of the Theoretically Possible Exploitation of Wind by Means of a Wind Motor." *Wind Engineering* Vol. 37 No. 4 (2013): pp. 441–446. DOI 10.1260/0309-524X.37.4.441.

[30] Molland, Anthony F., Turnock, Stephen R. and Hudson, Dominic A. *Ship resistance and propulsion: Practical es-*

Downloaded from asmedigitalcollection.asme.org/OMAE/proceedings-pdf/OMAE2026/89596/V010T14A005/7645839/v010t14a005-omae2026-175426.pdf by Deutsches Zentrum für Luft- und Raumfahrt (DLR) user on 19 October 2026

 Copyright © 2026 by ASME; reuse license CC-BY 4.0

timation of ship propulsive power. Cambridge Univ. Press, Cambridge (2011).

[31] Schwedt, Thorben, Gosala, Dheeraj, Lampe, Tobias, Fitz, Annika, Teske, Travis, Stutz, Sophie, Schmitz, Lars, Gosala, Vaidehi, Klein, Marco and Ehlers, Sören. "Enabling Energy Savings for Wind-Assisted Cargo Vessels Through Route and Speed Optimization." ASME (ed.). *OMAE 2026*. 2026.

[32] ITTC. "Practical Guidelines for Ship CFD Applications: ITTC 7.5-03-02-03 - Recommended Procedures and Guidelines." (2014). URL https://ittc.info/media/4196/75-03-02-03.pdf.

[33] ITTC. "Practical Guidelines for Ship Resistance CFD: ITTC 7.5-03-02-04 - Recommended Procedures and Guidelines." (2021). Accessed 2025-03-04, URL https://www.ittc.info/media/9775/75-03-02-04.pdf.

[34] Siemens Digital Industries Software. "Simcenter STAR-CCM+ 2410 - User Guide." (2024).

[35] Muzaferija, m. S., Peric, M., Sames, P. and Schelin, T. "A two-fluid Navier-Stokes solver to simulate water entry." *Twenty-Second Symposium on Naval Hydrodynamics*. 1998.

[36] Menter, F. R. "Two-equation eddy-viscosity turbulence models for engineering applications." *AIAA Journal* Vol. 32 No. 8 (1994): pp. 1598–1605. DOI 10.2514/3.12149.

[37] Kume, Kenichi, Hasegawa, Jun, Tsukada, Yoshiaki, Fujisawa, Junichi, Fukasawa, Ryohei and Hinatsu, Munehiko. "Measurements of hydrodynamic forces, surface pressure, and wake for obliquely towed tanker model and uncertainty analysis for CFD validation." *Journal of Marine Science and Technology* Vol. 11 No. 2 (2006): pp. 65–75. DOI 10.1007/s00773-005-0209-y.

[38] Yang, Xiao, Yin, Yong and Lian, Jingjing. "A numerical study on flow field and maneuvering derivatives of KVLCC2 model at drift condition." *Journal of Marine Engineering & Technology* Vol. 20 No. 1 (2021): pp. 52–63. DOI 10.1080/20464177.2019.1680076.

[39] Nachtane, Mourad, Tarfaoui, Mostapha, el moumen, Ahmed, Saifaoui, Dennoun and Benyahia, Hamza. "Design and Hydrodynamic Performance of a Horizontal Axis Hydrokinetic Turbine." *International Journal of Automotive and Mechanical Engineering* Vol. 16 (2019): pp. 6453–6469. DOI 10.15282/ijame.16.2.2019.1.0488.

[40] Hazim, S., El Ouatouati, A., Taha Janan, M. and Ghennioui, A. "Performance of a hydrokinetic turbine using a theoretical approach." *Energy Reports* Vol. 6 (2020): pp. 317–324. DOI https://doi.org/10.1016/j.egyr.2019.08.062. URL https://www.sciencedirect.com/science/article/pii/S2352484719305827. The 6th International Conference on Energy and Environment Research - Energy and environment: challenges towards circular economy.

[41] Marten, David. "QBlade: a modern tool for the aeroelastic simulation of wind turbines." DOI 10.14279/DEPOSITONCE-10646.

[42] Marten, David, Saverin, Joseph, Behrens de Luna, Robert and Perez-Becker, Sebastian. "QBlade Documentation v 2.0.9.6." (2024). Accessed 22.12.2025, URL https://docs.qblade.org/#footcite-marten2020.

[43] Marten, D., Paschereit, C. O., Huang, X., Meinke, M., Schröder, W., Müller, J. and Oberleithner, K. "Predicting Wind Turbine Wake Breakdown Using a Free Vortex Wake Code." *AIAA Journal* Vol. 58 No. 11 (2020): pp. 4672–4685. DOI 10.2514/1.J058308.

[44] Jonkman, B. J. *Turbsim User's Guide: Version 1.50*. Office of Scientific and Technical Information (OSTI) (2009). DOI 10.2172/965520.

[45] Branlard, E. "OpenFAST Toolbox." (2025). Accessed 22.12.2025, URL https://github.com/OpenFAST/python-toolbox.

[46] Tillig, Fabian and Ringsberg, Jonas W. "A 4 DOF simulation model developed for fuel consumption prediction of ships at sea." *Ships and Offshore Structures* Vol. 14 No. sup1 (2019): pp. 112–120. DOI 10.1080/17445302.2018.1559912.

Downloaded from asmedigitalcollection.asme.org/OMAE/proceedings-pdf/OMAE2026/89596/V010T14A005/7645839/v010t14a005-omae2026-175426.pdf by Deutsches Zentrum für Luft- und Raumfahrt (DLR) user on 19 October 2026

Copyright © 2026 by ASME; reuse license CC-BY 4.0